ADVANCED ENGINEERING MATERIALS
www.aem-journal.com

Strain-Hardening Behavior in an AA6060-T6 Alloy Processed by Equal Channel Angular Pressing

Tarek Khelfa, Jairo-Alberto Muñoz-Bolaños, Fuguo Li,* José-María Cabrera-Marrero, and Mohamed Khitouni*

Strain hardening is a useful mechanism for improving mechanical properties in materials. This study investigates the strain-hardening behavior of an AA6060 alloy processed by equal channel angular pressing (ECAP) up to 12 passes. Analysis by electron backscattered diffraction (EBSD) shows that the average geometrically necessary dislocations (GNDs) density increases continually up to the fourth pass and then saturates at a value of $\approx 1.85 \times 10^{14}$ m^{-2}. Hollomon and Kocks–Mecking–Estrin (KME) analysis are used to investigate the strain-hardening behavior of the resulting ultrafine-grained alloy. Results indicate that the strain-hardening capacity (H_C) and the strain-hardening exponent (n) of all deformed specimens are lower in comparison with the as-received condition. Moreover, the strain-hardening rate fluctuates with the ECAP passes. First, it increases from the first ECAP pass up to the fourth pass, then diminishes up to the fifth pass, and finally, it increases again with further deformation. The difference in the strain-hardening behavior of the ECAPed AA6060 is examined in terms of the grain size effect. It is shown that the strain-hardening curves change notably with diminishing the grain size. In addition, the KME model is used to depict the storage and annihilation of dislocations in the ECAPed specimens.

1. Introduction

Severe plastic deformation (SPD) techniques have attracted research interest as an efficient way to refine microstructures, thus enhancing the mechanical properties of metals and alloys.[1,2] One of the most popular and feasible SPD methods is the so-called equal channel angular pressing (ECAP). ECAP has shown a huge capacity for producing ultrafine grain (UFG) materials, making them very attractive to materials scientists.[3,4] In this technique, an intense plastic strain is imposed into the sample by repetitive pressing into a die consisting of two channels with equal cross-sections intersecting at an angle Φ.[5]

On the other hand, aluminum alloys of the AA6000 series have great potential in aircraft, aerospace, and automotive applications due to their low density, good corrosion resistance, good formability, and low cost.[6] In these particular alloys, both precipitation strengthening and work hardening are significant contributors to strength,[7] enabling Al alloys to substitute steel in the body-in-white and several structural components of the automobiles industry.[8,9]

In the last decades, many research works have reported favorable results of Al and its alloys processed by ECAP to obtain high strength while keeping good ductility.[10,11] However, most of the high-strength Al alloys after ECAP suffers from a decreasing strain-hardening capacity and thus the apparition of early necking under tensile deformation conditions.[12–14] Therefore, their elongation to failure is usually close to 5–10%, and the uniform deformation range is lower.[12,13] Moreover, the rapid process of dynamic recovery in Al alloys leads to reach an early steady-state dislocation density which does not facilitate strain hardening.[14,15] 6060-T6 is a precipitation-hardened Al alloy with relatively high contents of Mg and Si. Such alloying elements lead to strengthening via precipitation hardening by creating precipitates based on Mg and Si through

Dr. T. Khelfa, Prof. F. Li
State Key Laboratory of Solidification Processing
School of Materials Science and Engineering
Northwestern Polytechnical University
Xi'an 710072, China
E-mail: tarekkhelfa@yahoo.fr, tarekkhelfa@nwpu.edu.cn; fuguolx@nwpu.edu.cn

Dr. T. Khelfa, Prof. M. Khitouni
Laboratory of Inorganic Chemistry Ur-11-ES-73
Faculty of Sciences
University of Sfax
1171, 3018 Sfax, Tunisia

The ORCID identification number(s) for the author(s) of this article can be found under https://doi.org/10.1002/adem.202000730.

DOI: 10.1002/adem.202000730

Dr. J.-A. Muñoz-Bolaños
Department of Materials Science and Force Physics
National University of Science and Technology "MISIS"
Moscow 119049, Russia

Prof. J.-M. Cabrera-Marrero
Department of Materials Science and Engineering
Universitat Politècnica de Catalunya
EEBE-c/Eduard Maristany 10-14, 08019 Barcelona, Spain

Prof. J.-M. Cabrera-Marrero
Institute of Research in Metallurgyc and Materials
Universidad Michoacana de San Nicolás de Hidalgo
Edificio "U-3", Ciudad Universitaria, 58030 Morelia, Michoacán, México

solution heat treatment followed by subsequent artificial aging.[16] The sequence of precipitation in the AA6000 series is commonly known as supersaturated solid solution (SSSS) → Guinier Preston (GP) zones → β'' → β' → β (Mg_2Si).[16,17] Among these, the β'' precipitates are known to lead to the major strengthening contribution and therefore they are mainly responsible for the highest age-hardening effect.[16] However, it has been clearly found in recent investigation[18] that the β'' precipitates are shearable. In fact, X-ray diffraction (XRD) analysis revealed that the original AA6060-T6 alloy formed the following three intermetallic phases: Mg_2Si, and complex Al–Cu–Mg–Si and Al–Fe–Si phases.[16] Modeling and understanding the strain-hardening behavior of Al alloys is still more complicated than for single-phase alloys. Such complexity is attributed to the existence of precipitates and their associated distribution of the solute. Precipitates change the mean free path of dislocations. Many researchers[18–20] have studied the effect of the precipitates on the strain-hardening behavior of Al alloys under aging or deformation conditions (AA6063-T6, AA6061-T6, AA2195-T8, and AA2050-T34). Many practical methods have been developed to model strain hardening of metallic materials, including the simplistic one variable model proposed by Kocks–Mecking–Estrin (KME)[21] or models providing a more detailed definition of the microstructure.[22] Therefore, it is critical to enhancing their strain-hardening ability because it can help to retard the necking appearance (localized deformation) under tensile deformation[23] and hence raise the uniform elongation. According to Wang et al.,[14] the increased strain-hardening rates of UFG materials during deformation are related to the suppression of dislocation annihilation linked with thermally activated cross-slip and dislocations climb.

On the other hand, the accumulated strain and the generation of dislocation cells act as precursors of sub-grains, basically formed by low angle grain boundaries (LAGBs). According to some researchers,[24–26] with further deformation, LAGB can transform into high angle grain boundaries (HAGBs) as a consequence of continuous dynamic recrystallization (CDRX) phenomena from high geometrically necessary dislocations (GNDs) densities. Thus, a granular microstructure with average grain sizes smaller than ≈1 μm is finally obtained.[27–29]

GNDs are associated with gradients of plastic accommodation related to the average spacing of soft and hard areas during deformation distribution. Accordingly, a high capacity of storing more GNDs can increase the strain-hardening ability and consequently promote a good combination of strength and ductility.[30] This article aims to understand the effect of the ECAP process on the microstructural evolution and mechanical properties of an AA6060 alloy with a particular focus on their strain-hardening capacity and their ability to form GNDs.

2. Experimental Section

The current AA6060 alloy was supplied in T6 state in the form of extruded rods with a diameter of 10 mm. Its detailed chemical composition has been reported by Khelfa et al.[16] Rods were divided into cylinders having a length of ≈60 mm. ECAP was carried out using a die with two channels intersecting at an angle Φ of 90° with an external curvature angle Ψ of 37° (**Figure 1**a), corresponding to a theoretical strain of ≈1 per pass.[31] Deformation was performed at room temperature at a pressing speed of 0.02 m s^{-1}. Molybdenum disulfide (MoS_2) was used as a lubricant. Specimens were deformed up to twelve ECAP passes via route B_c.

The microstructures of the specimens were investigated by electron backscattered diffraction (EBSD) in a field emission gun–scanning electron microscope (FEG–SEM) ZEISS Ultra Plus SEM, operating at 20 kV. The EBSD data was studied using the HKL Channel 5 software. EBSD patterns were collected using different step sizes depending on the strain magnitude: 1.5 μm (zero ECAP passes), 0.1 μm (one pass, two passes, and three ECAP passes), and 0.08 μm (four, five, six, eight, and 12 ECAP passes). The grain sizes were determined by the line intercept method. LAGBs were considered for boundaries with misorientations ranging 2°–5° and 5°–15°, and plotted in red and green lines, respectively. However, HAGBs were considered for misorientations larger than 15° and plotted in blue. GNDs were obtained by MTEX toolbox software.

The microstructure images and EBSD analysis were taken on the transversal direction (TD) plane of the processed specimens, as shown in Figure 1a, where the axes of the reference system coincide with the extrusion direction "X" (ED), the normal direction "Y" (ND), and the transversal direction "Z" (TD). The specimens were mechanically polished from 2500 grit SiC paper till 0.02 μm colloidal silica suspension, followed by electropolishing in a 100 mL $HClO_4$ + 900 mL C_2H_5OH solution at −20 °C and a voltage of 20 V.

The mechanical properties were measured in the longitudinal direction by tensile tests using plane bone-shaped specimens having a gauge dimension of 6 mm (length) × 3 mm (width) × 2 mm (thickness). The tensile tests were carried out at room temperature in an INSTRON 5585H universal testing machine at a constant strain rate of 5.5×10^{-4} s^{-1}.

3. Results and Discussions

3.1. Microstructural Evolutions

Figure 1b shows the microstructure of the as-received alloy obtained by EBSD. This figure reveals a homogeneous distribution of equiaxed grains with a mean grain size of about 52 μm. In addition, Figure 1b demonstrates that HAGBs mainly form the initial grain boundaries. After one ECAP pass, Figure 1c shows a large amount of LAGB within the interiors of the original grains. It is also apparent that few fine grains with HAGBs appear along the original grain boundaries. As the deformation proceeds (i.e., the number of ECAP passes), the HABG fraction becomes higher by rising the misorientation angle. Therefore, Figure 1c–g highlights the LAGB fraction importance in the microstructure of the first six ECAP passes.

According to Estrin et al.,[32] this behavior can be attributed to the fact that during the first stages of SPD, new grain boundaries are created to subdivide the coarse grains into cell blocks. With deformations larger than six ECAP passes, Figure 1h–i exhibit that most of the LAGBs are transformed into HAGBs. According to Suresh et al.,[33] under the analyzed deformation conditions, the grains typically subdivide because of the creation

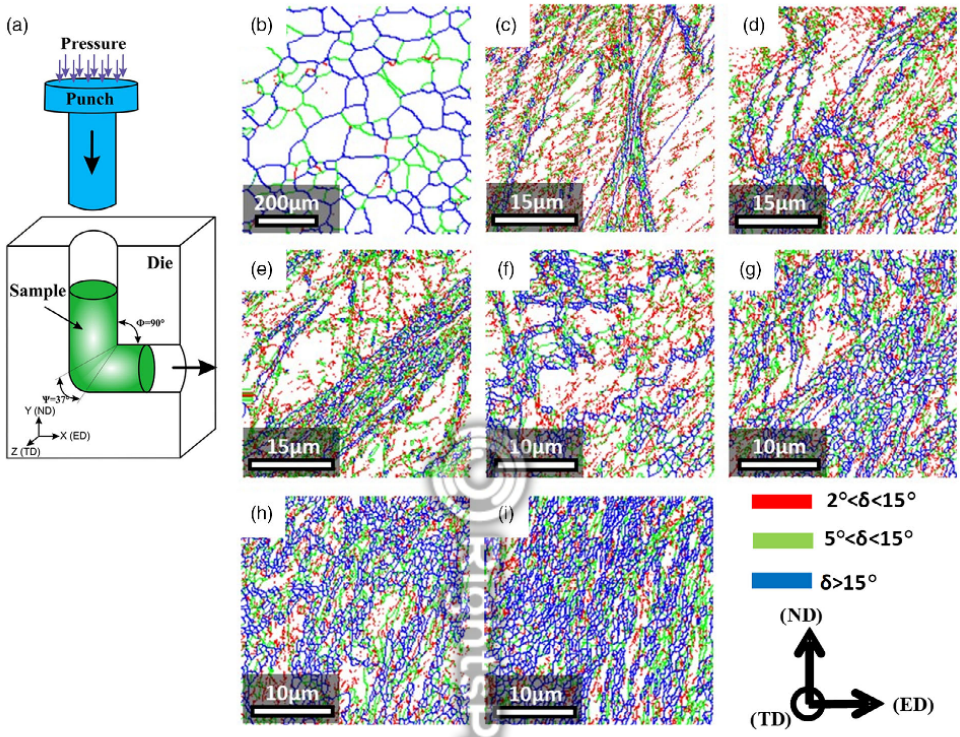

Figure 1. a) Schematic illustration of the ECAP process. Grain boundaries distribution in the ECAP samples; EBSD maps (HAGBs [misorientation > 15°] in blue and LAGBs, misorientation ranging 5°–15° in green and 2°–5° in red): Number of ECAP passes b) Zero; c) one; d) two; e) three; f) four; g) six; h) eight; i) twelve.

of deformation bands, where grain distortions create a contribution to increasing HAGBs fraction with more significant deformations. In addition, Humphreys and Hatherly[34] pointed out that grain boundaries with HAGB character also evolve during deformation, leading to a fine-grained microstructure formed by new small grains surrounded by HAGBs. In consequence, the grain size is gradually refined.

Figure 2 shows the misorientation distributions as a function of the number of ECAP passes. The HAGBs fraction is about 60.9% in the unprocessed material (Figure 2a), and it decreases to 17.95% after the first ECAP pass (Figure 2b). Then, the HAGBs fraction continually increases until 53.15% after 12 ECAP passes (Figure 2c–h). The slow variation of HAGBs fraction in the current alloy can be attributed to the delay of the recovery rate (in turns associated to the solute atoms content), which impedes new HAGBs to be created.[35] Figure 2g–h highlights the appearance of small peaks in the high-misorientation angle region between 50°–60°. This observation confirms that more LAGBs have evolved into HAGBs at a higher number of ECAP passes following specific orientations.

Different grain internal statistical methods can help to better describe grain size and grain boundaries evolution. For instance, the grain average misorientation (GAM) method calculates the average misorientation value inside each grain and establishes it as the overall value for the analyzed grain.[36,37] Because the dislocation densities in the deformed and recrystallized grains are quite different, the separation of recrystallized grains from deformed grains can be evaluated using GAM. This observation is based on the fact that dislocations in deformed grains form cellular structures that result in local misorientations of various degrees inside the grains. Conversely, recrystallized grains have much lower dislocation densities creating low internal grain misorientations.

Through **Figure 3**a–e, the change in GAM values is manifested with the deformation increase. Initially, Figure 3a shows that the as-received material registers GAM values between 0.4° and 1° (blue tones). After the first and fourth passes, Figure 3b,c demonstrate an evident change in the color of the grains, indicating a higher degree of deformation as well as the appearance of small blue grains inside the coarse grains. With the largest deformations, Figure 3d–e show that there is a mixture of small grains (blue color) and larger grains with high GAM values.

In the present work, the threshold values to separate recrystallized from deformed grains were defined considering the lower and upper limits of the as-received material distribution where a significant fraction of grains is not observed. According to

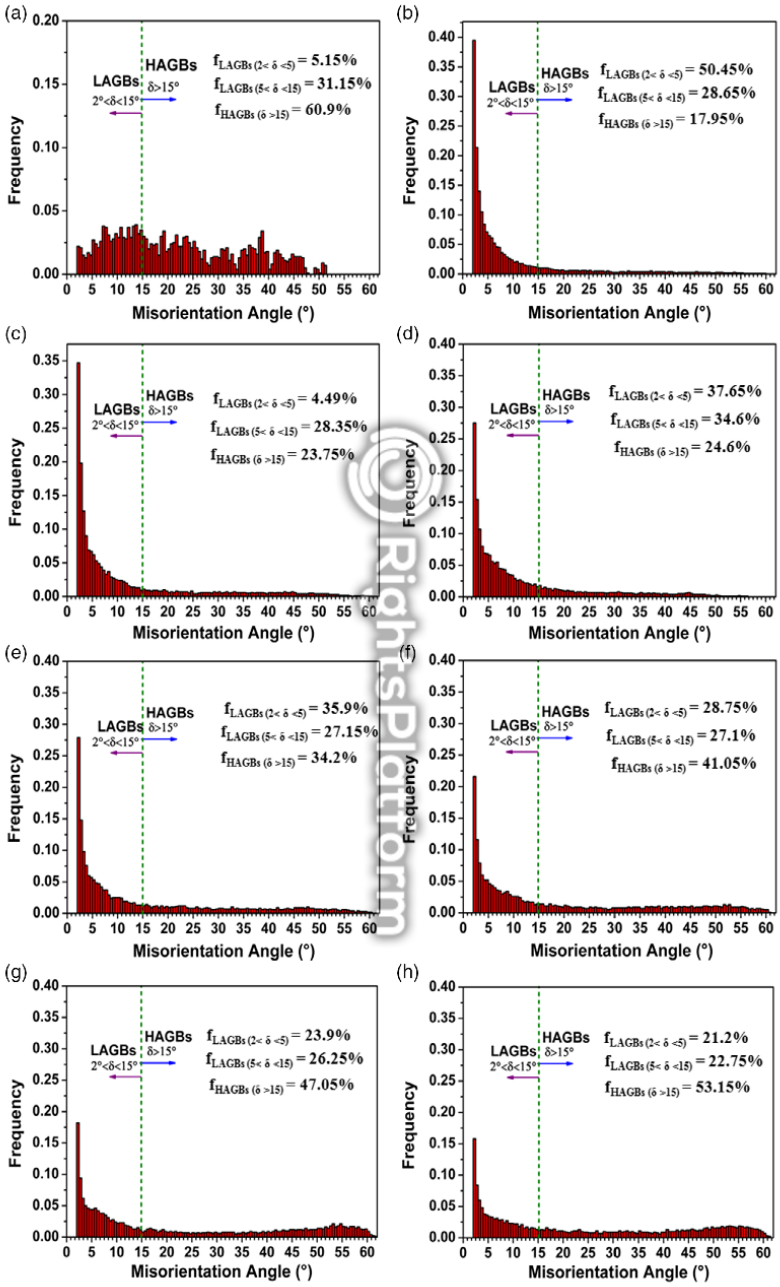

Figure 2. Distribution of misorientations of AA6060 before and after ECAP passes: a) Zero; b) one; c) two; d) three; e) four; f) six; g) eight; h) twelve.

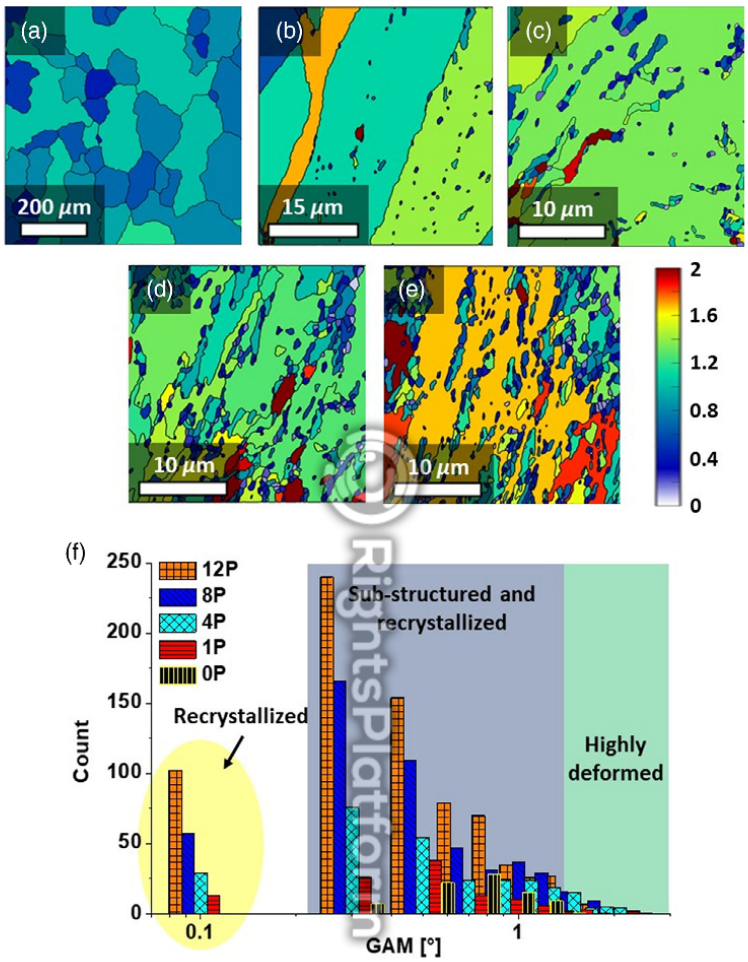

Figure 3. GAM representation for the material processed by a different number of ECAP passes: a) Zero; b) one; c) four; d) eight; e) twelve, and f) GAM plots.

the GAM distributions in Figure 3f, it is clear that GAM values of the as-received material range between 0.5°–1°. Hence, GAM values higher than 1° represent the deformed grains. In contrast, GAM values lower than 0.4° represent well the recrystallized state.

At first glance, Figure 3f shows different regions according to the GAM values. Around GAM values of 0.1°, there is a growing population of grains with the number of ECAP passes. These grains correspond to the small blue grains in the shear direction inside the original grains after the SPD process. This behavior demonstrates clear evidence of CDRX giving rise to microstructure regeneration with small grain sizes. Furthermore, Figure 3f also demonstrates a considerable fraction of deformed and substructured grains, especially for materials processed by ECAP. These observations indicate further grain refinement potential for the alloy, either through more ECAP passes or through the use of another deformation technique after ECAP.

3.2. Hardness Measurements

Figure 4a shows the microhardness evolution with the number of ECAP passes. At the beginning of ECAP processing, a steep hardness increase can be noticed up to the second ECAP pass. The microhardness increased from 92 HV in the as-received specimen to 113 HV after two ECAP passes. By applying further deformation, the microhardness increment is less evident, leading to a steady-state behavior. According to Gashti et al.,[38] the hardness saturation is due to the balanced competition between

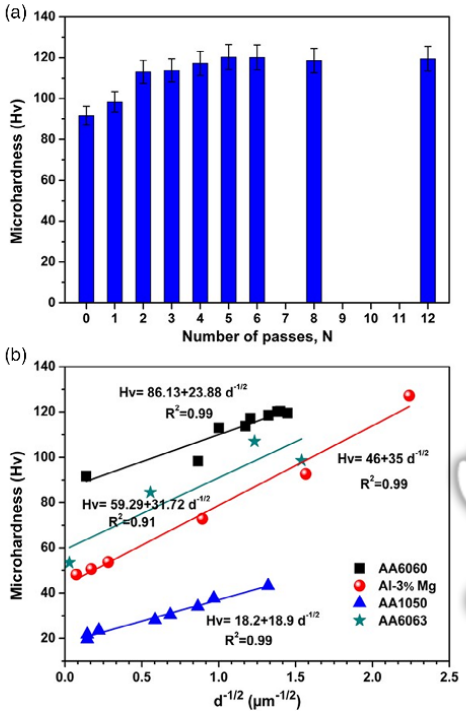

Figure 4. a) The variation of microhardness as a function of ECAP passes number for AA6060 samples and b) Hall–Petch plots (microhardness vs reciprocal square root of grain size) of aluminum alloys showing the comparison of present data with the results.

grain refinement and accumulation—annihilation of dislocations during deformation.

It has been demonstrated that hardness (HV) evolution follows a Hall–Petch relation with the grain size (d)[39]

$$\mathrm{HV} = \mathrm{HV}_0 + K_H d^{-1/2} \quad (1)$$

where HV_0 and K_H are the appropriate constants related to the hardness measurements. Figure 4b plots experimental HV against the reciprocal square root of the average grain size ($d^{-1/2}$) for the current alloy AA6060. For comparison purposes, other Al alloys, namely AA1050,[40] AA6063,[41] and Al-3%Mg[42] deformed by SPD are also included. It is readily apparent that only the Al-3%Mg alloy ($K_H = 35\ \mathrm{HV}\,\mu\mathrm{m}^{1/2}$) presents a higher slope than the other alloys. The Hall–Petch equation values for the Al alloys AA1050; AA6060, AA6063, and Al-3%Mg are 18.9, 23.88, 31.72, and 35 $\mathrm{HV}\,\mu\mathrm{m}^{1/2}$, respectively. In other words, the K_H value increases with high Mg content. According to Armstrong et al.,[43] the dislocations locked by Mg solute atoms generally generate a noticeable change to a higher slope in Al-Mg alloys.

3.3. Tensile Properties

Figure 5a shows the engineering stress–strain curves of the current AA6060 before and after ECAP. The ECAPed specimens display higher strength but lower ductility than the as-received specimen. Figure 5b summarizes the yield strength (YS), ultimate tensile strength (UTS), and elongation to failure. After the first ECAP pass, the alloy exhibits a sharp increase in the strength values. The YS and UTS change from about 171 and 244 MPa in the as-received specimen to 310 and 319 MPa after one ECAP pass. At subsequent ECAP passes, a gradual increase in tensile strength until five passes is noticed. Thereafter, the material reaches a saturation state.

In contrast to the material strength, the elongation to failure decreased from 25% to about 16% after the first ECAP pass. By increasing the ECAP passes, the elongation to failure gradually increases until the fifth ECAP pass, and then it remains nearly constant at about 20%. The initial elongation reduction can be associated with strain-hardening capacity.[44] However, the ductility increase at higher ECAP passes can be associated with the occurrence of recovery and continuous recrystallization, as previously demonstrated by the GAM analysis.[45–47] Similar results have also been reported in AA1050,[38] and AA1100 alloys[48] processed by accumulative roll bonding (ARB).

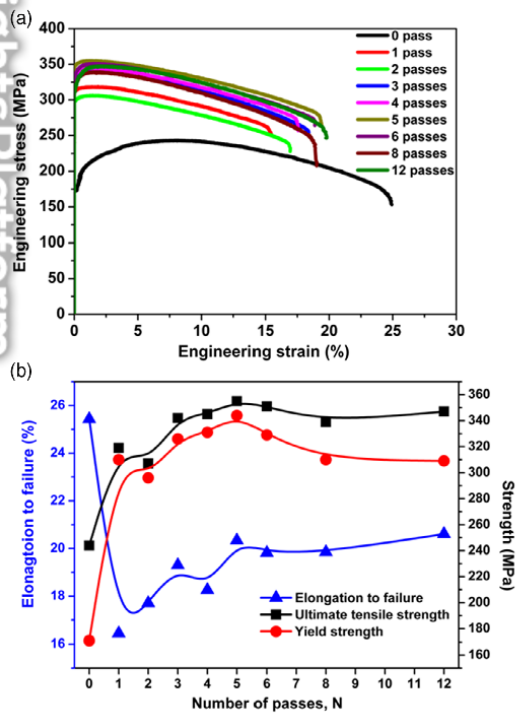

Figure 5. a) The engineering stress–strain curves and b) the variation of tensile strength and elongation to failure of undeformed and ECAPed AA6060 samples at different ECAP passes.

3.4. Stored Energy

From the thermodynamic viewpoint, the stored energy in grain boundaries and dislocations helps to understand the microstructure and mechanical properties of the UFG materials. Through the EBSD data, the stored energy due to the grain boundaries (E_b) can be assessed using the following equations[49]

$$E_b = S_V \bar{\gamma} = \frac{2\bar{\gamma}}{d_{\mathrm{ECD}}} \tag{2}$$

$$\bar{\gamma} = \sum_{2}^{62.8} [\gamma(\theta_0) f(\theta_0)] \tag{3}$$

$$\gamma(\theta) = \begin{cases} \gamma_m & \text{if } \theta_0 \rangle \theta_m \\ \gamma_m \left(\frac{\theta_0}{\theta_m}\right)\left[1 - \ln\left(\frac{\theta_0}{\theta_m}\right)\right] & \text{if } \theta_0 \langle \theta_m \end{cases} \tag{4}$$

Here, γ is the grain boundary energy for the entire grain structure, $f(\theta_0)$ represents the boundary fraction for a given orientation, γ_m is the energy per unit area of HAGB taken as 0.324 J m^{-2} for aluminum,[50] θ_m is considered as 15° and d_{ECD} is the mean equivalent circle diameter of the measured grains.

On the other hand, the stored energy due to dislocations E_d can be derived from the dislocation density measurements applying the following equation[34]

$$E_d = \frac{1}{2}\rho G \mathbf{b}^2 \tag{5}$$

where G is the shear modulus (26 GPa for aluminum), $\mathbf{b}$ is the Burgers vector (0.286 nm in aluminum), and ρ is the dislocation density.

Table 1 summarizes the E_b and E_d results. It is clear that the E_b increases with the amount of deformation; however, some oscillations occur in the fifth ECAP pass. This general behavior was explained by Higuera-Cobos and Cabrera[49] based on the grain size variations promoted by partial recrystallization. On the other hand, Table 1 reveals that the smallest sub-grain sizes were observed after the 5th and 12th pass, with values of $d_{\theta \geq 2^\circ} = 0.42$ µm, and $d_{\theta \geq 2^\circ} = 0.41$ µm, respectively. For that reason, it is worth mentioning that the highest values obtained at these stages (i.e., 5 and 12 ECAP passes), are an indication of the presence of a nucleation process of new grains.

Table 1. Values of boundary energy (E_b) and dislocations energy (E_d).

ECAP passes	$d_{\theta \geq 2^\circ}$ [µm]	$\bar{\gamma}$ [J m^{-2}]	E_b [J g^{-1}]	HAGB [%]	Dislocation density [m^{-2}][16]	E_d [J g^{-1}]
0	51.29	0.598	0.008	60.90	1.00×10^{12}	3.95×10^{-4}
1	0.95	0.444	0.34	17.95	1.14×10^{15}	0.44
2	0.74	0.462	0.46	23.75	1.29×10^{15}	0.5
3	0.57	0.482	0.62	24.60	1.07×10^{15}	0.42
4	0.54	0.495	0.67	34.20	1.17×10^{15}	0.46
5	0.42	0.529	0.92	46.20	9.60×10^{14}	0.38
6	0.43	0.517	0.70	41.05	9.30×10^{14}	0.37
8	0.49	0.522	0.78	47.05	1.06×10^{15}	0.42
12	0.41	0.546	0.97	53.15	9.10×10^{14}	0.36

The high and continuously increasing E_b values can be explained by two additional factors: 1) the high amount of LAGB even after 12 ECAP passes giving rise to high GNDs, and 2) the sub-grain size that decreases with deformation. In this order of ideas, Gholinia et al.,[51] also reported that the nonsaturation of grain size in Al-based alloys deformed by ECAP up to 16 passes was the main factor for the high E_b.

Conversely, Table 1 highlights that the dependence of the stored energy due to dislocations (E_d) on the ECAP passes follows a different behavior. The dislocations energy (E_d) increases until the 2 passes and then slightly decreases up to 5 passes, from where it seems to saturate around 0.37 J g^{-1}. The E_d decrease can be associated with recovery phenomena that lead to the statistically stored dislocation (SSD) annihilation. This observation is in good agreement with the E_d values of an AA6082-T6 alloy deformed by ECAP under warm processing conditions[52] where recovery took place. Thus, the high E_b values favor the grain size fragmentation, whereas the low E_d after the fourth ECAP pass seems to influence the strength decrease.

3.5. GND Densities Evolution

As already stated, the EBSD analysis can be used to determine the GNDs density.[25] The scalar GND density (ρ_{GND}) can be calculated dividing the Nye's tensor (α) norm by the Burgers vector[29]

$$\rho_{\mathrm{GND}} = \frac{1}{\mathbf{b}} \sqrt{\alpha_{ij}\alpha_{ij}} \tag{6}$$

Figure 6 represents the GNDs density maps for undeformed and deformed samples. Although the undeformed material shows some places with high GNDs densities (Figure 6a), the maximum density sites of GNDs are randomly distributed inside of some grains. The maximum GND is 8.95×10^{13} m^{-2}, whereas the average value is 3.92×10^{12} m^{-2}. It is noticeable in Figure 6b that after one ECAP pass, the highest GND densities locate inside the sheared grains, more specifically where sub-grains appear. This behavior is in correspondence with the more significant fraction of LAGBs in this deformation stage. Figure 6c–e demonstrates that with increasing strain, GNDs slightly increase following the same path of the one ECAP pass material, but with small grain size. Figure 6f shows that the GNDs distribution curves move toward major values with high ECAP passes. However, the average GNDs density after four passes keeps quite similar and independent on the ECAP passes. This GND saturation reflects that the ECAP process has reached its lower limit for the grain size reduction in this alloy. Muñoz et al.[53] mentioned that the high GNDs in UFG materials measure the capacity to reach smaller grain sizes. In this way, high GND gives rise to grains subdivision that helps to compensate for the curvature induced by the SPD. In addition, Figure 6g records the SSDs (calculated by XRD[16]), and the average GNDs. In the same way that energy contributions evolved, average SSDs increase with the first two passes and then slightly decrease up to six passes from where stabilization was noticed, whereas the GNDs keep a growing evolution with strain. This rise of GNDs in UFG material suggests that there is a great probability of further reduction in grain size, considering that GNDs are responsible for the grain subdivision.[54] LAGBs evolution has the same tendency as GNDs

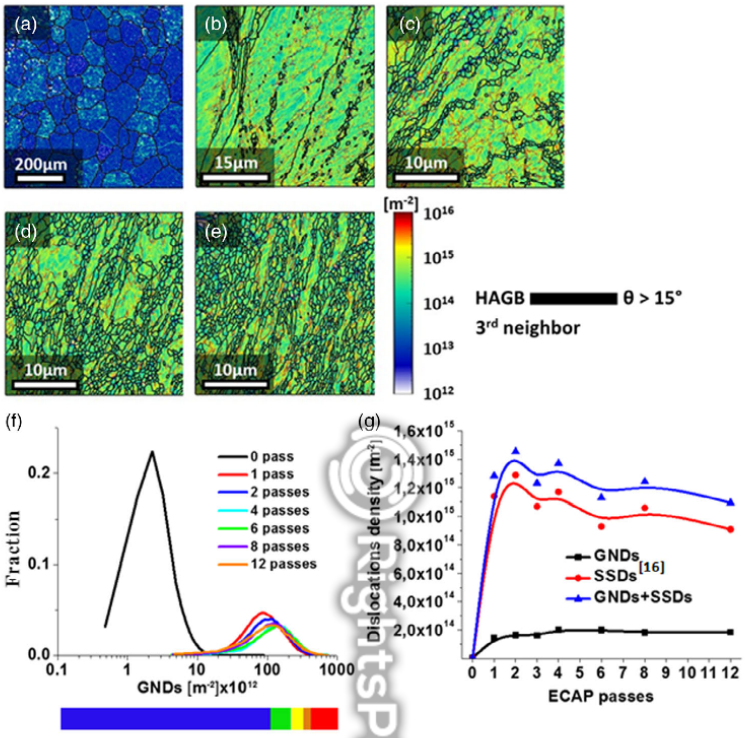

Figure 6. GNDs density maps before and after different ECAP passes: a) zero; b) one; c) four; d) eight; and e) twelve. f) Graph summarizing calculated values of GND fractions, and g) dislocations density calculated using ESBD and XRD[16] techniques.

because the GNDs are due to the contribution of two components, mainly known as curvature-induced dislocations (CIDs) that build disorientation across dislocation cell walls, where the later component depends on the subgrain size and LAGB misorientation. On the other hand, the SSDs values are about six times higher than GNDs. However, these observations prove the huge grain size reduction (GNDs evolution) as well as the strength decrease after 6 ECAP passes (SSDs evolution). The difference in quantity is a consequence of the distinct kind of dislocations calculated through the used characterization techniques (GNDs and SSDs).

3.6. Strain-Hardening Behavior

Material hardening capacity (H_c) can be defined as the ratio between the UTS (σ_{UTS}) and the yield stress (YS (σ_y)). Afrin et al.[55] recharacterized the hardening capacity by a normalized parameter as

$$H_C = \frac{\sigma_{UTS} - \sigma_y}{\sigma_y} = \frac{\sigma_{UTS}}{\sigma_y} - 1 \quad (7)$$

Table 2 shows the hardening capacity of ECAPed specimens after different passes. One can see that the H_c values decrease from 0.426 (initial specimen) to 0.029 after one ECAP pass, followed by a gradual increase until attaining a value of 0.123 after twelve ECAP passes. The H_c variation corresponds well with the grain refinement, and dislocation densities variation with the

Table 2. The values of strain-hardening exponent (n) and strength coefficient (k) of the investigated AA6060 samples based on the Hollomon analysis.

ECAP passes	Strain-hardening capacity [H_C]	Strain-hardening exponent [n]	Strength coefficient [k MPa]
0	0.426	0.109	348
1	0.029	0.011	338
2	0.037	0.012	326
3	0.049	0.015	370
4	0.042	0.013	370
5	0.031	0.008	372
6	0.066	0.018	384
8	0.093	0.022	377
12	0.123	0.032	401

ECAP passes. In consequence, the lower the dislocations increments, the more reduced the strain-hardening capacity.

To better understand the ductility evolution after ECAP processing, special attention was paid to the strain-hardening behavior. For this purpose, the Hollomon equation was fitted to the experimental flow curves[56]

$$\sigma = k\varepsilon^n \tag{8}$$

Here, σ, ε, k, and n represent the true stress, true strain, the strength coefficient, and strain-hardening exponent, respectively.

Figure 7a allows differentiating the data between undeformed and ECAPed specimens. In addition, Table 2 summarizes the strain-hardening exponent (n) and strength coefficient (k) of the undeformed and ECAPed specimens. The strain-hardening exponent for the undeformed alloy is $n \approx 0.11$. However, after ECAP processing until the fifth ECAP pass, the strain-hardening exponent values decrease and fluctuate between 0.008 and 0.015. Then, with more than five ECAP passes, the n values slightly grow, ranging between 0.018 and 0.032. The continuous changes in the exponent n after ECAP processing can be attributed to the evolution of the microstructural characteristics. For example, the large fractions of subgrains in the initial stages of deformation (<5 passes) that hinder the movement of dislocations within the grains affects the strain-hardening capacity. The situation changes with more than 5 passes, because the conversion of LAGB into HAGB favors the movement of dislocations within the smaller grains, giving rise to small increases in the exponent n.

For a better understanding of the alloy strain-hardening capacity, Figure 7b exhibits a Kocks–Mecking type plot of strain-hardening rate θ as a function of net flow stress $(\sigma - \sigma_y)$ at different ECAP passes. Figure 7b highlights that the strain-hardening rate θ in stage III for the as-received material starts instantly after reaching the yield stress. This stage is distinguished by a linear decrease with the flow stress and indicates a value of $\theta = 3101$ MPa. Then, stage IV appears, and the strain-hardening rate goes down progressively.

As shown in Figure 7b, in stage III hardening, the crossing point of the slope lines (θ against $(\sigma - \sigma_y)$) with $(\sigma - \sigma_y) = 0$ represents the value of stage III hardening θ_0^{III}. The slope of the curves, $\beta = -\frac{d\theta}{d\sigma}$, is called the dynamic recovery rate.

Figure 7b and **Table 3** collect the values of θ_0^{III} and β. It can be seen how the values of θ_0^{III} increase considerably (values of θ_0^{III} between 4000 and 13 000 MPa) with deformation by ECAP. These values demonstrate that the deformed material hardens quickly. However, due to the small space for the dislocation motion, these materials cannot maintain the hardening at large strains. For this reason, deformed materials lead to early necking formation. On the other hand, Table 3 demonstrates that the magnitude of β values increases after the deformation process.

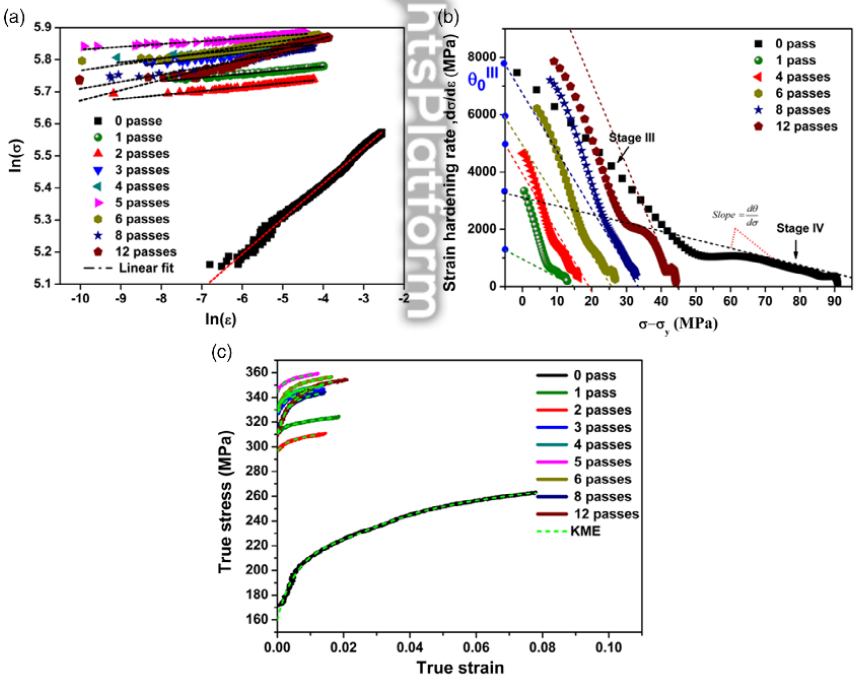

Figure 7. a) The ln σ versus ln ε plots for analyzing of strain-hardening behavior (the Hollomon analysis) of unpressed and ECAP-ed AA6060 samples; the slope of the line segment is equivalent to n value, b) evolution of strain-hardening rate with stress $(\sigma - \sigma_y)$ of as-received and ECAPed AA6060 alloy, and c) KME model and experiment of AA6060 in different ECAP passes.

Table 3. The values of (θ_0^{III}, β) and (k_1, k_2) of the investigated AA6060 samples based on Kocks–Mecking type plots and KME model, respectively.

ECAP passes	θ_0^{III}	$\beta = -\frac{d\theta}{d\sigma}$	k_1	k_2
0	3101.24	−31.46	2.36×10^9	92.70
1	1222	−70.27	1.23×10^{10}	415.00
2	1887.76	−81.42	1.11×10^{10}	458.91
3	3996.57	−207.15	1.50×10^{10}	518.94
4	4431.73	−271.96	1.36×10^{10}	508.97
5	4089.43	−295.88	1.58×10^{10}	681.31
6	6437.57	−244.20	1.20×10^{10}	493.69
8	7427.46	−216.58	1.08×10^{10}	490.30
12	13 806.28	−321.64	7.71×10^9	374.94

The β values evolution demonstrates that the alloy after ECAP processing experiment a major dynamic recovery rate. In this sense, the strength decrease, and the elongation improvement after 4 ECAP passes are explained by the high dynamic recovery rates obtained in these deformation stages.

To examine deeper the strain-hardening behavior, dislocations, precipitation, solid solution, dislocations, and grain size strengthening mechanisms were all taken under consideration, as indicated by[57]

$$\sigma = \sigma_0 + \sigma_{HP} + \sigma_d + \sigma_{SS} + \sigma_{preci} \tag{9}$$

where σ_0 is a friction stress contribution, $\sigma_{HP} = kd^{-1/2}$ is the Hall–Petch contribution, σ_{SS} is the solid solution strengthening of the alloying elements in the aluminum matrix, σ_{preci} is the precipitation strengthening, and $\sigma_d = M\alpha Gb\rho^{1/2}$ is the Taylor dislocation contribution where M is the Taylor factor, α is a constant, G the shear modulus, **b** the Burgers vector, and ρ is the total dislocation density. Using the Hall–Petch relation ($\sigma_y = \sigma_0 + K_H d^{-1/2}$), Equation (9) can be rewritten as[57]

$$\sigma \approx \sigma_y + \sigma_d + \sigma_{SS} + \sigma_{preci} \tag{10}$$

Afterward, the stress contribution linked to the dislocation density (ρ) can be determined by subtracting σ_y from the overall flow stress as[57]

$$\rho^{1/2} \propto \sigma_d \approx (\sigma - \sigma_y - \sigma_{SS} - \sigma_{preci}) \tag{11}$$

Using the KME strain-hardening model, the grain size effect on strain hardening was studied. This model depicts the relationship between the dislocations storage rate and dislocation density (ρ), and it can be written as[22]

$$\frac{d\rho}{d\varepsilon} = k_1\rho^{\frac{1}{2}} - k_2\rho \tag{12}$$

where the first term $k_1\rho^{\frac{1}{2}}$ accounts for the statistical storage of dislocations, and the second term $-k_2\rho$ is related to dynamic recovery phenomena.

Figure 7c shows the experimental and predicted values of true stress–strain curves for all the analyzed conditions obtained by the KME model. The tensile curves predicted from the KME model (dashed line) correlated well with the experimental curves (solid line) for both as-received and deformed materials. Table 3 indicates the different KME model parameters. It is apparent that the k_1 values in ECAPed specimens are approximately one order higher than in the as-received specimen, suggesting a smaller mean free path or a higher capacity to store dislocations (i.e., high dislocation densities).

In contrast, the k_2 values in ECAPed specimens are higher than for the as-received specimen, which indicates the most active dynamic annihilation and recovery mechanisms operating during deformation in the ECAed specimens. According to Changela et al.,[58] in an arbitrary dislocation structure, dislocations are much more easily eliminated when dislocations are not well-organized forming stable cell arrangements. Table 3 allows observing that k_2 increases until the fifth pass and then decreases to reach stabilization at strains higher than six ECAP passes. Accordingly, the early instability in the UFG alloy is associated with the increase in k_2 values that induce recovery leading to material softening.

4. Conclusion

From the present results, it can be concluded that: 1) A strain-induced continuous reaction based on the dislocation motion leads to the transformation from LAGBs to HAGBs and the gradual diminution of the cell which is essentially similar to a CDRX. 2) When increasing the ECAP passes number, both yield and tensile strength rose significantly and reached about 344 and 355 MPa after 5 passes, respectively. In contrast to the strength, the elongation to failure decreased from about 25% for the as-received specimen to about 16% for one ECAP pass specimen. By increasing the strain, these values gradually increase until five ECAP passes and then remained nearly at a constant value of about 20%. The increase in ductility can be attributed to the occurrence of recovery and continuous recrystallization. 3) The stored energy increases with strain up to five ECAP passes and then diminishes with a trend toward stabilization. The decrease in the stored energy is due to the evolution of new fine grains and recovery process. The slight increase in the stored energy at high deformation levels is due to the production of new dislocations. 4) The average GNDs density reached saturation after the fourth ECAP pass. This saturation may be attributed to the dynamic equilibrium reached among multiplication and annihilation of dislocations. At the same time, the SSDs are ≈6 times greater than GNDs. 5) A remarkable increase in strain-hardening rate during initial passes of ECAP results in the fact that with rising deformation, the HAGBs fraction rises. During tensile testing, HAGBs act as dislocation sinks and provide more deformation and therefore rising strain-hardening rate. 6) The predicted stress–strain curves from the KME model correlated well with the experimental results. The results show that the decrease in the softening term in the KME model in the alloy after 6 ECAP passes, explains the increase in ductility.

Acknowledgements

T.K. and F.L. acknowledge the financial support of the National Natural Science Foundation of China (Grant No. 51275414, No. 51605387). The authors thank Fundació CTM (Centro Tecnológico de Manresa) for

